Corrosion of Electrogalvanized Steel in 0.1 M NaCl

Studied by SVET

A.C. Bastos, A.M. Simões[*], M.G. Ferreira[a)]

Departamento de Engenharia Química, Instituto Superior Técnico, Av. Rovisco Pais, 1049-001 Lisboa, Portugal

[a)]Departamento de Engenharia de Cerâmica e do Vidro, Universidade de Aveiro, Aveiro, Portugal

Abstract

The corrosion of electrogalvanized steel exposed to 0.1M NaCl was studied using the SVET. Situations of localized corrosion, cathodic protection and corrosion protection due to surface pre-treatment were analyzed, putting in evidence the possibilities of the technique.

Keywords: corrosion, galvanized steel, localized corrosion, SVET, zinc.

Introduction

The electrochemical techniques commonly used to study corrosion phenomena give information on the current and potential of the working electrode in an electrochemical cell. In spite of their tremendous importance, those values refer to the whole area of the electrode and do not give information on the distribution along the electrode's surface. This is particularly important for cases of localized corrosion such as pitting, interstitial, intergranular or galvanic corrosion. In recent years several techniques have been developed with the capability of determining distribution maps of quantities such as current densities [1-4], Volta

---

[*] Corresponding author. E-mail: alda.simoes@ist.utl.pt

potential [5-8], and ion concentrations (such as H^+) [2,9-10]. In this work, a technique that measures local current densities, the Scanning Vibrating Electrode Technique (SVET), was used to study the corrosion of electrogalvanized steel.

The SVET technique

The SVET was first developed and used by biologists to study ionic fluxes in biological systems [11-13], having been applied to the corrosion field in the 70's with the pioneering work of Isaacs [14-16]. Since then the instrumentation has received several developments that have increased its intensity (detecting currents down to nanoamperes), ease of operation and ease of data analysis. The technique measures local current intensities at active metal surfaces immersed in electrolyte solutions. It is based on the measurement of the extremely small potential variations that exist in solution due to the fluxes of ionic currents originated by the electrochemical reactions that occur on the active surface. In a corroding surface, oxidation and reduction often take place in separated regions, of variable number and size. In these regions, and according to the nature and rate of each reaction, ions are formed and distributed in solution, with concentration gradients that create electric fields. Such potential gradients can be detected using a microelectrode that measures the potential difference among points all over the surface and a standing second microelectrode that works as reference. Fig.1 shows schematic representations of the potential and current distribution in the solution above an active metal surface. To increase the sensitivity, the microelectrode is made to vibrate, transforming the measured signal into an a.c. signal with the same frequency as the vibration. A lock-in amplifier filters all signals of other frequencies, reducing noise to a great extent.
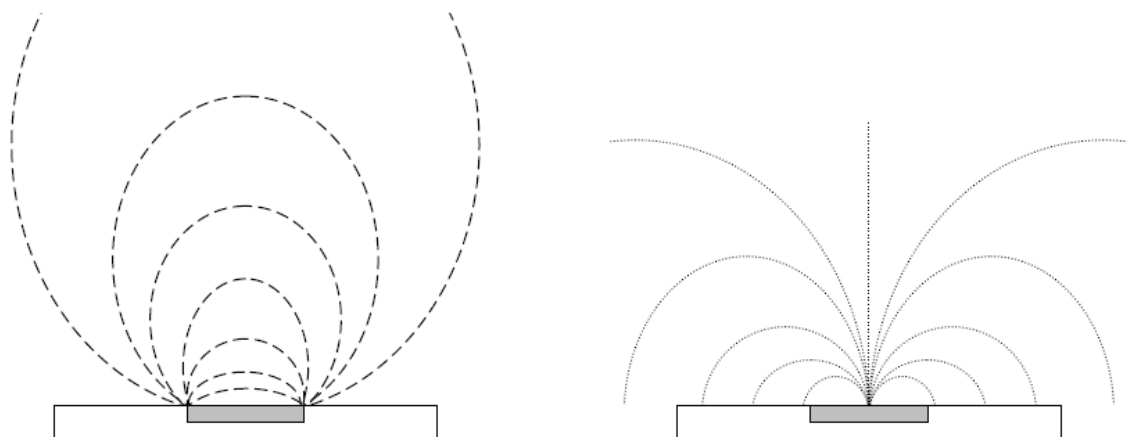
Figure 1. Schematic representations of a local corrosion cell showing equipotential surfaces (left) and current lines (right). The central rectangle represents an anode whereas the sides are considered cathodic [adapted from ref.1].

A map of current distribution can be obtained making a grid of points and measuring in each point the potential difference while scanning in a plane parallel to the surface of the sample. The potential (*V*) measured in each point can be related [1] to the current intensities (*I*) of the processes occurring at the metal surface by Ohm's Law, using eq. (1).

$$V = \frac{I\rho}{2\pi d} \tag{1}$$

where ρ is the solution resistivity and *d* the distance between the point of measurement and the source of the current. To accurately use the values acquired by the system, calibration is done by placing the vibrating microelectrode at a known distance from another microelectrode, source of a given constant current. Fig. 2 shows a schematic representation of the current that flows from the tip of the microelectrode, as well as the equation that gives the current values at a given distance from a point current source [17- 19]. The calibration is valid for the solution used and while the amplitude and the frequency of the vibration remain unaltered [15].
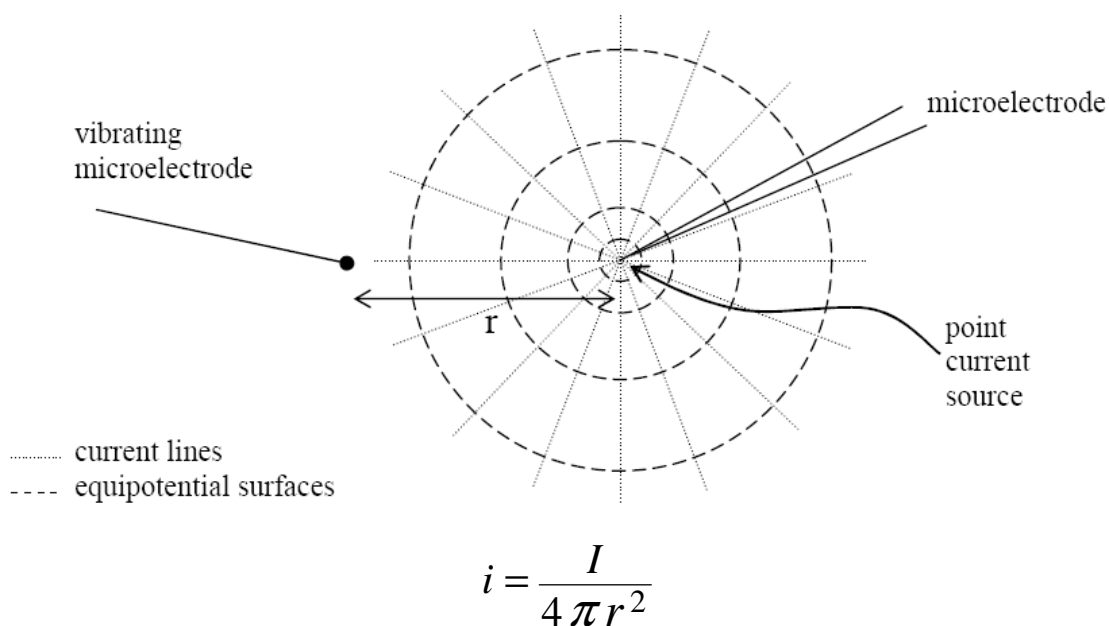
$$i = \frac{I}{4\pi r^2}$$

Figure 2. Schematic representation of microelectrode tip used as a point current source for calibration. The equation gives the current i that should be measured at a distance r from the source of current I [17].

Experimental

Samples

Commercial electrogalvanized steel (EG) with and without pre-treatment was used (Fig. 3). The steel thickness was 800 µm and its composition is presented in Table 1. The electroplated zinc layer had a nominal thickness of 7 µm. The pre-treatment consisted of phosphatation followed by a chromate rinse. The samples were ultrasonically cleaned for 5 minutes with acetone, followed by distilled water and then dried with compressed air. Samples of 1x1 cm were glued to an epoxy cylinder (sample support) of 1 cm height and 1.5 cm radius. Adhesive tape with a cut window of 2 x 2 mm was used to delimit the area to be studied. Adhesive tape was also applied around the epoxy support to form a solution reservoir (Fig. 4). The samples were exposed to 0.1 M NaCl, at room temperature. The solution was prepared using p.a. grade salt and distilled water.
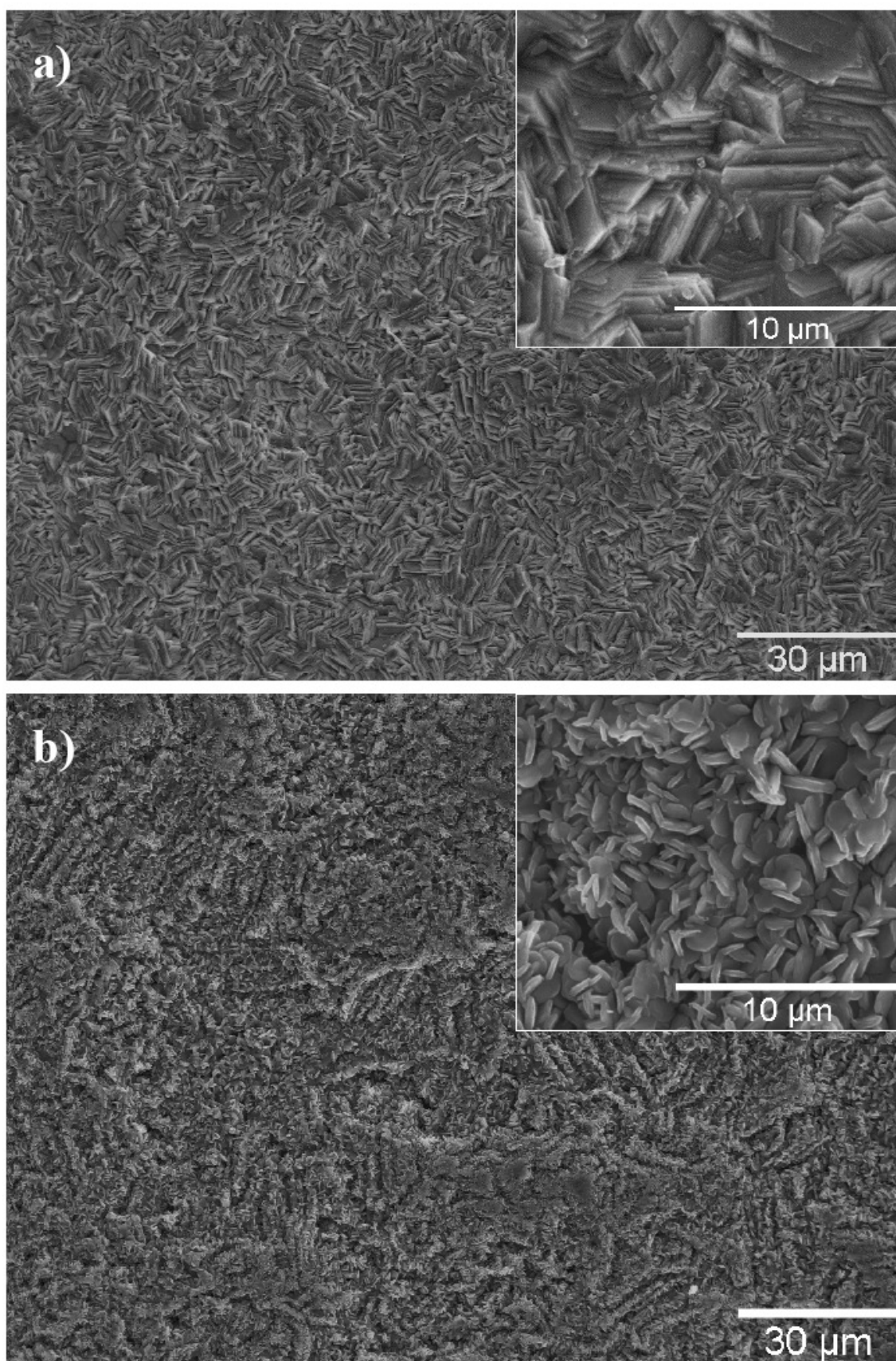
Figure 3. Micrographs of the electrogalvanized steel (a) and the phosphated electrogalvanized steel (b).
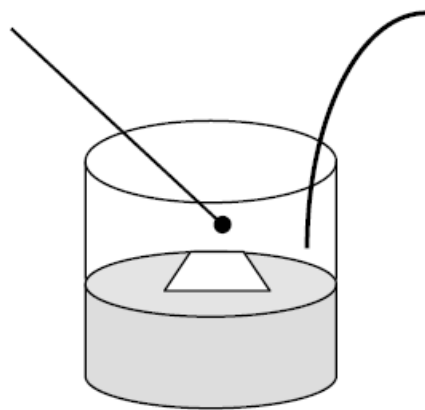
Figure 4. Representation of the sample glued to the epoxy support with adhesive tape forming the solution reservoir. Above the sample, the vibrating microelectrode (left) and a platinum black wire reference electrode (right) are observed.

Table 1. Steel analysis as given by the manufacturer (weight %).

C	Si	Mn	P	S	Al	N
0.0035	0.0090	0.1120	0.0125	0.0060	0.0340	0.0032

Cu	Cr	Ni	Ti	Nb	Fe
0.0095	0.0200	0.0150	0.0625	0.0015	balance

Measurements

The SVET instrumentation was manufactured by Applicable Electronics Inc. [18] and controlled by the ASET program developed by Sciencewares [19]. The microelectrodes (Micro Probe Inc. PI200101F), Pt/Ir (80%/20%) wires insulated with paralene C$^{®}$ and arced at the tip to expose the metal, were platinized to form a small spherical platinum black deposit of 10-20 μm diameter. The position of the probe was software controlled by means of stepper motors that permitted discrete 1 μm precision movement in each of the 3 axes. An additional motor controlled a video camera that collected real time images of the sample. The system measured the electric field in two directions, normal and parallel to the surface. The double vibration of the probe was set by two piezoelectronic wafers driven by sine wave oscillators and the signals from both vibrations were filtered by two lock-in amplifiers.

The measurements were made with the electrode tip vibrating at 200 μm above the surface, with frequencies in the order of 200-400 Hz, and 20-30 μm of

amplitude. In each scan 21x21 points were recorded for an exposed area of 2x2 mm. The acquisition time in each point was 0.2 s with 0.1 s of waiting time between points to minimize the perturbation induced by the translation of the microelectrode. Each scan took 5 minutes and started with an image acquisition of the surface and a reference measurement with the microelectrode apart from the active area to measure the signal of the solution without any activity. This value was subtracted from the values measured during the scan. After immersion scans were taken every 15 minutes for the first 3 hours, then every hour for the first day and finally every day until the end of the experiment.

Data treatment

The experimental data were converted to local current densities. The values in each point are presented as a vector with an orientation and magnitude correspondent to the direction and modulus of the current. A vector upwards means anodic current (positive) and a vector downwards means cathodic current (negative). A map of these vectors is a set of arrows that can be overlaid onto the image of the surface, showing the current in each point of the sample and giving a picture of the corrosion status at the moment of that particular scan. Various scans recorded at various exposure times permit to follow the progress of the corrosion process.

Surface Analysis

A Hitachi S-2400 Scanning Electron Microscope coupled to a Rontec Energy-Dispersive X-Ray Spectrometer (EDS) was used to study the surface morphology. The EDS system used detects elements with atomic number above 11 (Na), thus oxygen and carbon are not detected, which is an important limitation of the technique.

Results and Interpretation

Figs. 5 to 7 show distribution maps of local current densities and surface images obtained at different immersion times, for each of the samples studied.
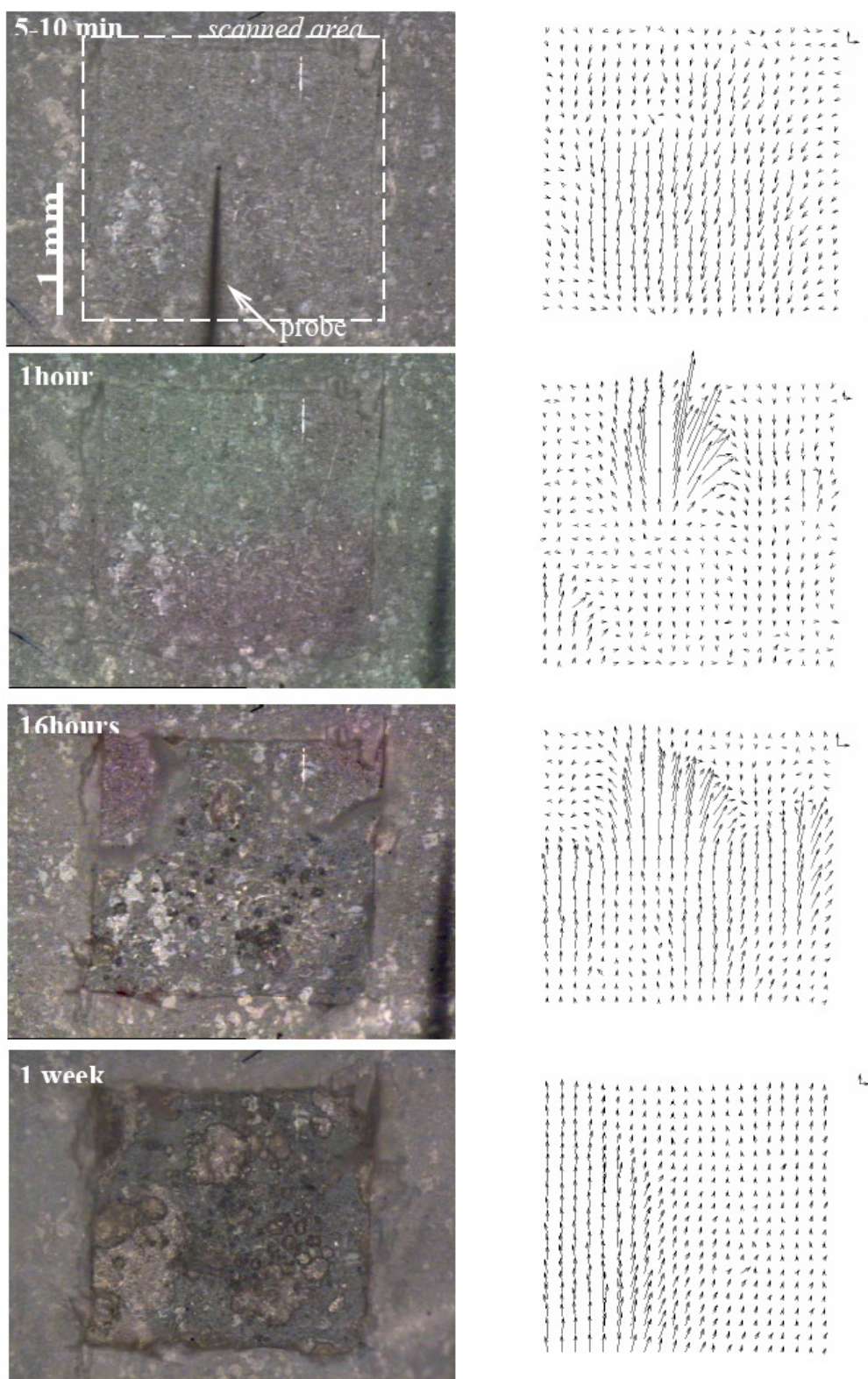
Figure 5. Optical images and current density maps of electrogalvanized steel exposed to 0.1M NaCl at different immersion times. On the top right of each map a two vectors scale corresponds to $10\mu Acm^{-2}$ in each direction.
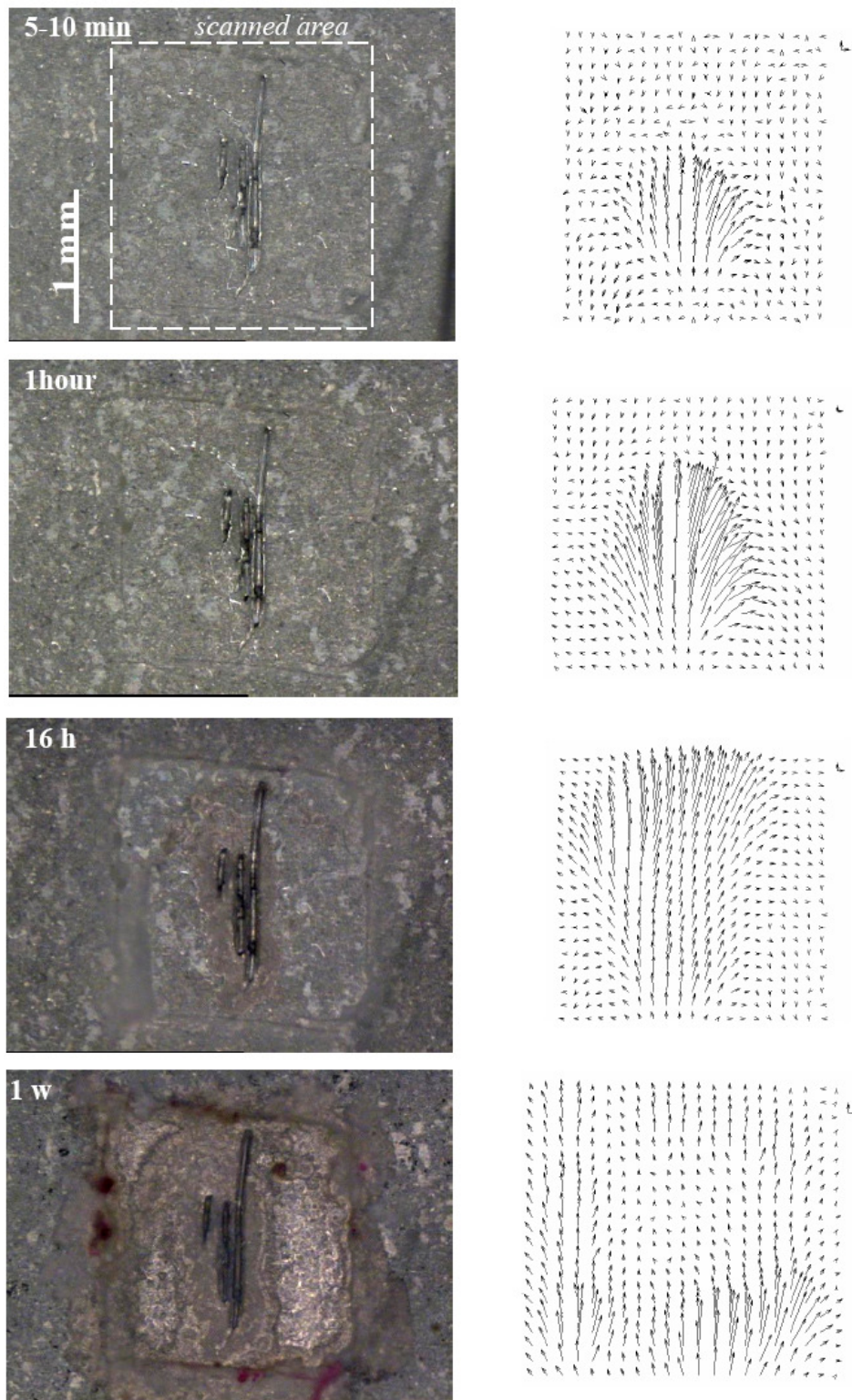
Figure 6. Optical images and current density maps of electrogalvanized steel with a defect exposed to 0.1M NaCl, at various immersion times. On the top right of each map a two vectors scale corresponds to $10\mu Acm^{-2}$ in each direction.
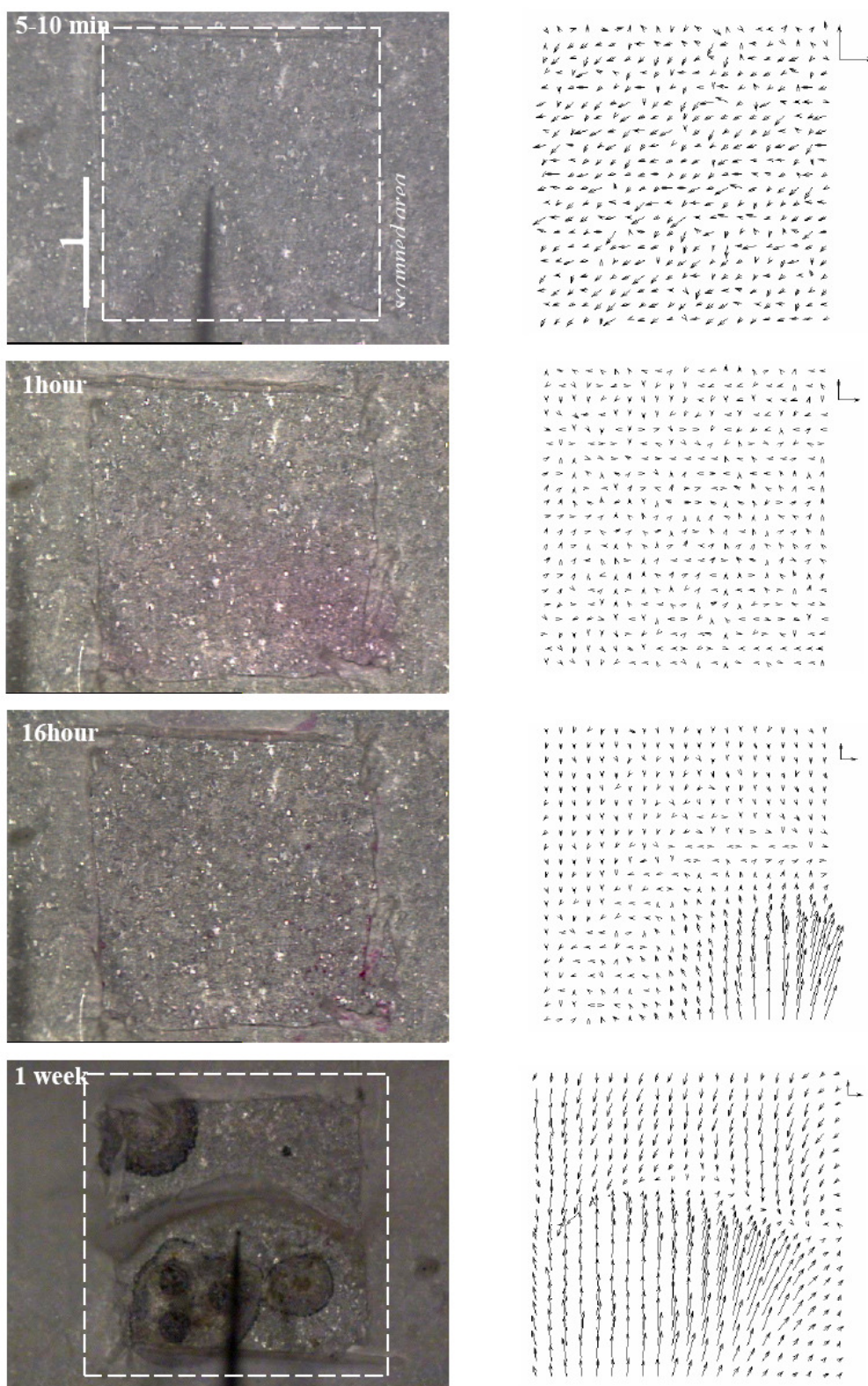
Figure 7. Optical images and current density maps of a phosphated electrogalvanized steel exposed to 0.1M NaCl at various immersion times. On the top right of each map a two vectors scale corresponds to $10\mu Acm^{-2}$ in each direction.

For the corrosion of EG (Fig. 5), a small activity, predominantly cathodic, was observed in the first minutes of immersion. After 1 hour of immersion, strong anodic activity became apparent in one localized area, whereas after 16 hours the anodic currents had extended to a larger area, possibly due to depassivation of the areas originally covered with air-formed oxides. In the upper corners of the image taken at 16 hours it was possible to observe corrosion products on the border of both anodic and cathodic regions. The final map was taken after a week and shows moderate activity, predominantly anodic.

For the scribed EG sample, Fig. 6, anodic activity was detected since the beginning of immersion. After one hour the magnitude of the anodic current increased significantly and the anodic area was also larger. After 16 hours, anodic activity continued to dominate the map, covering most of the area with strong currents. One week later, the surface revealed shinny metallic areas, together with orange/brown spots, corresponding to iron corrosion products. The activity measured by the SVET was mainly anodic and concentrated at the limits of the adhesive tape. The evolution of the system can be explained, in a first stage, by the influence of the scribe, where the metallic zinc and possibly some iron had become exposed. After that, activation and dissolution of the zinc along the surface occurred, increasing the anodic area. Since the zinc cathodically protected the iron areas, the anodic reaction also became faster and, given the small thickness of the zinc layer, zinc quickly became dissolved, leaving a larger area with iron exposed. At the end of the experiment most of the surface consisted of steel, consequently the cathodic protection was no longer efficient and iron started to corrode locally. For the phosphated EG (Fig. 7), no activity was detected in the first hours of immersion. The 16 hours scan showed oxidation only in one small part of the substrate and the video image of the sample revealed a surface without any signs of attack. The results after one week of exposure show that a considerable extension of the surface remained unattacked. White corrosion products are observed in the boundary that separates the anodic from the cathodic region.

Comparison of the three samples reveals that in the first minutes of immersion only the scribed sample showed strong activity, whereas the phosphated revealed no activity. At the end of experiment the phosphated sample showed significant area still unattacked, in contrast with the other two samples, for which the zinc coating had practically disappeared. Iron corrosion products appeared in the scribed sample, the one that was more severely corroded.

Fig. 8 was obtained with an EG sample after 24 hours of immersion and it clearly shows the localized attack – Fig. 8a). A close look at one pit – Fig. 8b) –allows the identification of three regions: the zinc layer that surrounds the pit, the pit itself (that corresponds to the steel exposed by localized dissolution of zinc) and the center of the pit with corrosion products. The same three regions can be observed in more detail in a scanning electron micrograph – Fig. 8c). Identification made by X-ray microanalysis has shown the difference between the various regions, some with zinc only, others with iron only (in the center of the pit), and finally the presence of zinc, iron and some chloride in the regions of the corrosion products, suggesting the presence of zinc hydroxychlorides. This is in agreement with the literature [20-24], where descriptions of hydroxychlorides and carbonates were found.

Discussion

The results concerning the corrosion of zinc can be interpreted based on the literature. Graedel [20] gives a review of corrosion mechanisms for zinc exposed to the atmosphere, whereas Suziki [21] and Verkatesan [22] studied the corrosion products of zinc in chloride media. According to those authors, zinc is always covered by a zincite layer, ZnO, and, depending on the environment humidity, zinc hydroxide, $Zn(OH)_2$, may also be present. The presence of carbon dioxide converts some of the zinc hydroxide to a complex hydrated zinc carbonate/zinc hydroxide mixture. In the present results, the small activity in the first minutes of immersion for EG sample can be explained by the existence of this layer of oxides and hydroxides spontaneously formed during atmospheric zinc exposure, which acts as a protective barrier, preventing corrosion. The immediate activity

observed for the scribed samples is explained by the destruction of this barrier in the defect. Moreover, the existence of exposed steel increases the rate of zinc oxidation in the process of cathodic protection.

One interesting observation was that zinc corrosion was always reasonably localized, i.e., it started at small areas and then it changed from site to site along the surface. Localized attack of zinc has been described by other authors [21-23]. In the absence of defects the corrosive process starts with the attack of the oxide barrier by the action of water and chloride ions and zinc oxidation occurs not in a uniform way, but in local cells with areas of roughly 0.01 to 0.5 mm^2 [23]. The results thus confirm that zinc oxidation starts locally in defined places, most likely in the vicinity of defects or inclusions, and proceeds both in depth and laterally, enlarging the active area. When steel is reached the oxidation continues in adjacent places. Steel does not corrode, provided there is enough zinc in its vicinity, but it starts to corrode at a later moment, when cathodic protection is lost. One interesting feature in this work was the formation of corrosion products in the frontier between the anodic and cathodic regions, when only zinc is exposed. This can be observed in the optical images for one week of immersion in Fig.7 and compared to the respective current map, or the 16 hours result in Fig. 5. The precipitation occurred where the $Zn^{2+}_{(aq.)}$ ions coming from the anodic region met a high concentration of $OH^{-}_{(aq.)}$ coming from the cathodic sites. When zinc ions reach points with a sufficiently high pH, they precipitate as $Zn(OH)_2$. The fact that precipitation starts in the vicinity of the cathodic areas, and not in other areas, suggests that zinc hydroxide may be the initial corrosion product, although the final composition of the corrosion products seemed to include hydroxychlorides and possibly carbonates.
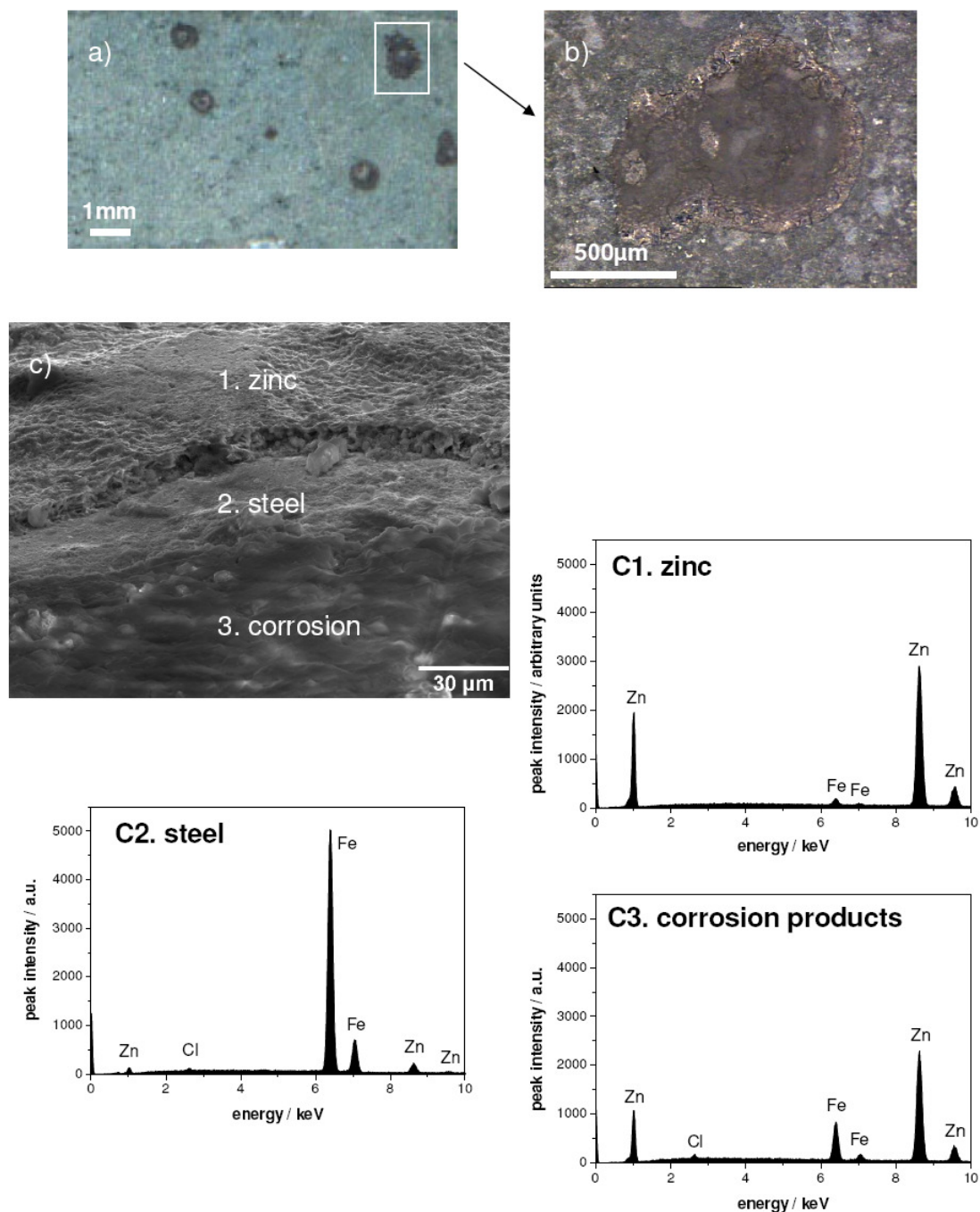
Figure 8. a) Micrograph of the surface of EG without pre-treatment after 1 day of exposure ; b) the same for a single pit; c) micrograph of the detail of a pit showing three distinct regions. X-ray microanalysis of the three regions in (c) are presented in C1, C2 and C3.

In the phosphated sample the corrosion process was delayed for some hours. Probably the phosphate crystals prevented the contact of the metal with the aggressive solution. The mechanisms for corrosion of phosphated zinc have been reviewed by Amirudin and Thierry [25]. It seems that even before corrosion onset, phosphate layers can become attacked by NaCl solutions, losing PO_4^{3-} or Zn^{2+} or both, depending on the pH. When corrosion occurs, low and high pH values are encountered in the anodic and cathodic sites, respectively, which is likely to enhance phosphate dissolution. Thus, possibly corrosion initiation occurred when the protective layer became destroyed, starting from regions that were more weakly covered than others. The phosphate dissolution was localized and in those regions corrosion proceeded as described for the other samples. After one week of immersion the phosphated samples showed active corroding areas, together with regions that remained protected by the phosphate layer

One problem in the results is the predominance of anodic or cathodic currents, apparently with no balance from the reverse reaction. In fact, some of the maps presented only reveal cathodic activity, whereas others depict only anodic areas. This is surprising, since only the scanned 2x2 mm area of the metal surface was exposed to the solution, which means that all the oxidation and reduction reactions should be restricted to that area, with both positive and negative currents balancing and being in principle detected by SVET. The reason for this unexpected result is not totally clear yet, but it may be due to the difference in current densities. In principle, a localized process is easier to detect, since it leads a higher current density, and thus to a local flux of ions, with high fields generated in the solution. In contrast, when one of the reactions spreads along a large surface, the current densities can be quite small, and thus the local currents may easily become too small to be detected. Another possibility, particularly in the cases where anodic activity is not observed, is the existence of interstitial corrosion at underneath the adhesive tape, with the exposed metal (in direct

contact with the dissolved O_2) acting as a cathode and the metal beneath the tape acting as anode.

Further work is needed in order to understand and overcome these problems. Nevertheless for qualitative or semi-quantitative observations SVET permits to observe and detect the changes that occur in the metal surface.

Conclusions

The results evidence the suitability of SVET for the study of the mechanism and spatial distribution of corrosive attack and illustrate the great potential of this new technique in many fields of corrosion research. Its capability to resolve local currents allowed following the corrosion process of different samples, during immersion in NaCl aqueous solution. The results have shown that:

     1 - Zinc oxidation started in localized regions, moving to adjacent areas when it became consumed in the previous sites.

     2 – After zinc consumption, the steel that became exposed remained cathodically protected by zinc.

     3 - The existence of a defect accelerated the corrosion process not only by destroying the protective oxide layer at the zinc surface, but also by exposing steel that has to be protected. This increased the zinc oxidation rate.

     4 - The phosphate layer retarded the onset of zinc corrosion and decreased the corrosion rate even after one week of immersion.

The great advantage of the technique is the spatial resolution, which makes it an excellent complement to the classical electrochemical techniques.

References

1. H.S. Isaacs, Y. Ishikawa, Applications of the Vibrating Probe to Localized Current Measurements, *in* Electrochemical Techniques for Corrosion Engineering, R. Baboian (Ed.), NACE, Houston, 1986.

2. K. Ogle, V. Baudu, L. Garrides, X. Philippe, *J. Electrochem. Soc*. 147 (2000) 3654.

3. R.J. O'Halloran, L.F.G. Williams, C.P. Lloyd, *Corrosion* 40 (1984) 344.

4. N. Hsu, J.D. Garber, R. Brunel, R.D. Braun, *Corrosion* 43 (1987) 606.

5. M. Stratmann, *Corros. Sci*. 27 (1987) 869.

6. M. Stratmann, H. Streckel, *Corros. Sci*. 30 (1990) 681.

7. S. Yee, R.A. Oriani, M. Stratmann, *J. Electrochem. Soc*. 138 (1991) 55.

8. A. Leng, H. Streckel, M. Stratmann, *Corros. Sci*. 41 (1999) 547.

9. J.O. Park, C.H. Paik, R.C. Alkire, *J. Electrochem. Soc*. 143 (1996) L174.

10. L. Changjian, Z. Xiangdong, D. Ronggui, F. Zude, paper 178, 7th International Symposium on Electrochemical Methods in Corrosion Research, Budapest, 2000.

11. A.M. Shipley, J.A. Feijó, The use of Vibrating Probe Technique to Study Steady State Extracellular Currents During Pollen Germination and Tube Growth, Chapter 17 *in* Fertilization in Higher Plants. Molecular and Citological Aspects. Springer-Verlag, 1999.

12. O. Bluh, B. Scott, *Rev. Sci. Inst*. 10 (1950) 867.

13. W.P. Davies, *Fed. Proc*. 25, Abstract 801 (1966) 332.

14. H.S. Isaacs, G. Kissel, *J. Electrochem. Soc*. 119 (1972) 1628.

15. H.S. Isaacs, *Corrosion* 43 (1987) 594.

16. H.S. Isaacs, *Corros. Sci*. 28 (1988) 547.

17. C. Sheffey, Electric Fields and the Vibrating Probe for the Uninitiated, in Ionic Currents in Development, A.R. Liss (Ed.), A.R. Liss Inc., 1986, p. xxv.

18. www.applicableelectronics.com

19. www.sciencewares.com

20. T.E. Graedel, *J. Electrochem. Soc*. 136 (1989) 193C.

21. I. Suzuki, *Corros. Sci*. 25 (1985) 1029.

22. R. Venkatesan, *Brit. Corros. J*. 33 (1998) 77.

23. E. Almeida, Corrosão Atmosférica do Zinco *in* Corrosão Atmosférica, Mapas de Portugal, E. Almeida, M. Ferreira (Ed.), INETI, Lisboa, 1998.

24. S.C. Chung, S.L. Sung, C.C. Hsien, H.C. Shih, *J. Appl. Electrochem*. 30 (2000) 607.

25. A. Amirudin, D. Thierry, *Prog. Org. Coat*. 28 (1996) 59.